Materials Advances

ROYAL SOCIETY OF CHEMISTRY

PAPER

View Article Online
View Journal

Cite this: DOI: 10.1039/d5ma00197h

Mechanochemical synthesis of poly(azomethine)s: a sustainable vehicle for metallic supports in valorisation of glycerol

Jean A. Medina, [ab] Angela Matarín,[a] Patricio A. Sobarzo, [c] Claudio A. Terraza [b] and Eva M. Maya *[a]

Received 4th March 2025,
Accepted 30th July 2025

DOI: 10.1039/d5ma00197h

rsc.li/materials-advances

A polymeric support based on a poly(azomethine) (PAM) structure was synthesized using mechanochemical polymerization (**PAM@M**) and compared with its counterpart prepared *via* conventional high-temperature solution-phase polycondensation (**PAM@T**). The mechanochemical approach not only significantly reduced the synthesis time (1 hour *versus* 24 hours), but also resulted in a polymer with amorphous character while the one synthesized *via* conventional heating exhibits some crystalline peaks. **FePAM@M** demonstrated superior catalytic performance with complete conversion of glycerol to solketal with 100% selectivity in only 1 hour at room temperature, exhibiting an impressive environmental factor (*E*-factor = 3.49). The conversion of glycerol into value-added products is essential due to its large-scale generation as a by-product of biodiesel, so the results of this work highlight **FePAM@M** as a highly efficient and sustainable catalyst for this valorisation.

Introduction

Aromatic poly(azomethines) (PAMs), also known as poly(imines) or Schiff base polymers, are highly interesting materials which are generally prepared *via* condensation between dialdehydes and diamines using a great variety of solvents and conditions: typically *via* high-temperature polycondensation using high polarity solvents such as dimethylacetamide or *m*-cresol using long reaction times (1–3 days)[1] or by using a mixture of *N*-methylpyrrolidone (NMP) and hexamethylphosphoramide (HMPA), in the presence of lithium chloride as water trap, stirring the mixture for 16–48 h at room temperature.[1,2] Taking this background into account, there is a need to find more sustainable and efficient procedures for the synthesis of this type of polymer. In this sense, our group has contributed to a more sustainable synthesis of these materials employing microwave radiation, reporting successful syntheses in shorter reaction time.[3,4]

Another powerful tool is mechanochemistry, which promotes chemical reactions induced by mechanical force, enabling bond breaking and formation without relying on heat, light or solvents typically required by using conventional methods.[5–9]

Thus, for example, mechanochemistry has been applied in the synthesis of pharmaceutical compounds,[10] for catalytic transformations,[11] organometallic synthesis,[12,13] fluorination reactions,[14] and even the construction of non-carbon covalent backbones such as phosphazanes (P–N)[15] as well as the synthesis of inorganic compounds.[16] Moreover, mechanochemical polymerization has enabled the synthesis of a wide range of linear and porous polymers and provides a versatile platform for post-polymerization modifications such as that of a AuNP-doped imine-COF catalyst.[17]

However, despite its many advantages, such as reduction or elimination of solvents, and the use of various types of monomers, even with low solubility, and shorter reaction times, this polymerization technique has hardly been used to synthesise aromatic PAMs. To the best of our knowledge, a few works have been reported where mechanochemical polymerization has been used to react a diamine with a dialdehyde.[17,18] Their low solubility and the abundance of metal-chelating sites provided by the nitrogen atoms in the imine bonds make PAMs an excellent choice for heterogeneous catalytic applications. Consequently, they have been widely studied and employed as heterogeneous catalysts in a wide range of processes such as selective dye degradation,[19] Suzuki coupling reactions,[20] CO_2 cycloaddition to epoxides[3,21,22] or oxygen reduction reaction.[23]

However, PAMs have not been used as heterogeneous catalysts for the conversion of glycerol into value-added compounds

[a] *Instituto de Ciencia de Materiales de Madrid, Consejo Superior de Investigaciones Científicas, Madrid, Spain. E-mail: eva.maya@csic.es*
[b] *Research Laboratory for Organic Polymers (RLOP), Facultad de Química y de Farmacia, Pontificia Universidad Católica de Chile, P.O. Box. 306, Post 22, Santiago, Chile*
[c] *Departamento de Polímeros, Facultad de Ciencias Químicas, Universidad de Concepción, Casilla 160-C, Concepción, Chile*

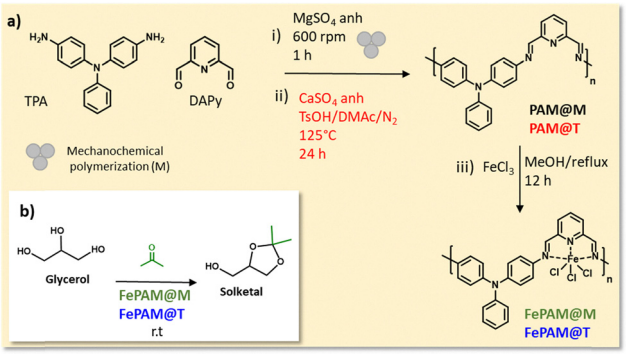

Fig. 1 (a) Synthesis of poly(azomethine)s *via* mechanochemical polymerization (i), high-temperature polycondensation in solution (ii), and synthesis of iron-loaded poly(azomethine) preparation (iii); (b) catalytic acetylation of glycerol into solketal.

which is a process of great interest since it is the main waste in the biodiesel production industry. In fact, for every 100 tonnes of biodiesel, 10 tonnes of glycerol are generated.[24,25] Its polyfunctional nature, characterized by three hydroxyl groups, enables a wide range of chemical modifications. These include its conversion into industrial chemicals such as acrolein, epichlorohydrin and glycolic acid, as well as its transformation into fuel additives such as glycerol derived ethers and esters. Additionally, it is used as a precursor for pharmaceutical applications, such as glycerol carbonate, which is widely used in drug production.[26–29] In addition, the conversion of glycerol *via* several catalytic processes aligns with several principles of green chemistry, as it promotes the use of renewable resources, reduces waste generation and uses catalysts to enhance conversion.[30]

Among glycerol-derived ethers, solketal (Fig. 1b) is emerging as a potential additive for oxygenated fuels that offers a sustainable alternative to petroleum-derived additives such as methyl *tert*-butyl ether (MTBE) and ethyl *tert*-butyl ether (ETBE).[31] Solketal is typically produced by acetylation of glycerol using acid catalysts, metal-based catalysts or bifunctional catalysts combining both acid and metal active centres[32–35] and, recently *via* photocatalysis.[36–38] Among the heterogeneous catalysts explored in this conversion, metal oxides and their catalytic complexes, molecular sieve catalysts and heteropoly metalate catalysts have been the most widely studied.[24–27] Thus, obtaining solketal from glycerol is not only an opportunity to obtain a sustainable additive, but it is also a way of recovering glycerol.

However, few heterogeneous polymeric catalysts have been reported for this reaction: some polymer-based coordination catalysts[39,40] a polyurethane,[41] copolymeric gels,[42] and anthracene[43] or quinone-based[38] porous organic polymers.

Most of the metal-based catalysts, both homogeneous and heterogeneous, including abundant elements such as iron and aluminium operate at 60–120 °C with reaction times of 1–6 hours.[44–47] The development of recyclable, non-toxic, iron-loaded catalysts operating at room temperature is a significant step towards sustainability.

Thus, in this work we have used mechanochemical polymerization (M) to prepare a novel PAM by reacting 4,4′-diaminotriphenylamine (TPA) with 2,6-pyridinedicarboxaldehyde (DAPy) (**PAM@M**, Fig. 1a). For comparative purposes, its counterpart, PAM **PAM@T**, has been synthesized using conventional high-temperature polycondensation reaction in solution (T). We have taken advantage of the presence of nitrogen atoms and the pincer-like structure adopted in both polymers to anchor iron from a solution of $FeCl_3$ obtaining iron-loaded polyazomethines, **FePAM@M** and **FePAM@T** (Fig. 1a).

In the second part of this work, we have employed both polymers, **FePAM@M** and **FePAM@T**, as heterogeneous catalysts in the valorisation of glycerol to obtain a high added value product, solketal (Fig. 1b).

Experimental

Materials

Aniline, anhydrous calcium sulfate ($CaSO_4$), cesium fluoride, 1-fluoro-4-nitrobenzene, *p*-toluenesulfonic acid monohydrate (TsOH) and anhydrous *N*,*N*-dimethylacetamide (DMAc) were purchased from Sigma-Aldrich. 2,6-Pyridinedicarboxaldehyde (Py) was acquired from AK Scientific, Inc. Dimethylsulfoxide (DMSO), methanol, hydrazine hydrate solution (80 wt%), and palladium on carbon (Pd/C, 10 wt%) were obtained from Merck. All reagents and solvents were used as received.

Monomer synthesis

4,4′-Diaminotriphenylamine (TPA) was prepared using a two-step reaction: a dinitro compound was synthesised and then reduced to TPA using hydrazine and 10% Pd/carbon as the catalyst according to the synthetic procedures described for this compound (see the SI).[48]

2,6-Pyridinedicarboxaldehyde (DAPy) was prepared following the procedure previously reported.[21]

Polymer syntheses

PAM@M. Pyridine-2,6-dicarbaldehyde (DAPy, 135 mg, 1 mmol), 4,4′-diaminotriphenylamine (TPA, 275 mg, 1 mmol) and anhydrous magnesium sulfate (60 mg, 0.5 mmol) were added to a zirconia vessel provided with three 2 cm diameter zirconium balls and placed in the planetary rotation mill. The vessel was subjected to a stirring speed of 600 rpm for 1 h, after which the material obtained was recovered, washed with water under stirring for 3 h. The solid was filtered under vacuum and dried in a vacuum oven at 110 °C for 24 h, yielding a dark brown solid (359 mg, 96%).

PAM@T. A two-necked flask was charged with pyridine-2,6-dicarbaldehyde (DAPy, 0.135 g, 1 mmol), *p*-toluenesulfonic acid monohydrate (TsOH; 45 mg, 0.24 mmol), anhydrous calcium sulfate (65 mg, 0.48 mmol), and dimethylacetamide (DMAc; 5 mL). The reaction mixture was heated to 60 °C for 30 min and then 4,4′-diaminotriphenylamine (TPA, 0.275 g, 1 mmol dissolved in 4 mL DMAc) was slowly added under a nitrogen flow and then 1 mL of DMAc was added. The reaction mixture was slowly heated to 125 °C and stirred for 24 h. The mixture was

then cooled to room temperature and then poured into water (100 mL), a precipitate was formed, and stirred for 3 h at room temperature. The precipitate was filtered under vacuum and washed with plenty of water. The solid obtained was dried under vacuum at 70 °C for 24 h and an orange solid was obtained (0.355 g; 95%).

Fe-based PAMs

In a 100 mL one-neck flask provided with a magnetic stirrer and a condenser, the corresponding polymer **PAM@M** or **PAM@T** (0.150 g, 0.40 mmol), anhydrous $FeCl_3$ (0.065 g, 0.40 mmol) and 50 mL of methanol were added. The mixture was heated under reflux for 20 h, after which it was allowed to cool to room temperature. The black solid obtained was filtered under vacuum, washed with THF and dried under vacuum at 110 °C for 24 h, yielding the corresponding iron-loaded PAMs as black solids, (**FePAM@M**) (202 g, 94%) and **FePAM@T** (155 g, 72%).

Catalytic activity

The following procedure is an example of how the assays were performed following the values depicted in Table 1.

Glycerol (0.18 mL; 2.5 mmol), acetone (0.84 mL; 11.41 mmol) and **FePAM@M** (8 mg; 0.4 mol% Fe) were added to a micro-reactor tube provided with a magnetic stirrer. The mixture was then stirred for a time period indicated in Table 1. The catalyst was separated from the solution *via* vacuum filtration or centrifugation and allowed to dry under vacuum at 110 °C. The liquid was analysed by gas chromatography. Glycerol conversion and solketal quantification were calculated based on a calibration curve (Fig. S1).

Table 1 Acetylation of glycerol (G) using poly(azomethines) based catalysts[a]

En.	Catalyst	No. of cycles	Time (h)	G Con. (%)	S Yield (%)	S/DMDO
1	FePAM@M	1	1	100	100	100/0
2		2	1	100	100	100/0
3		3	1	100	100	100/0
4		4	1	100	83	83/17
5		4	2.5	100	100	100/0
6		5	1	43	33.5	78/22
7		5	2.5	100	85	85/15
8		5	3.5	100	85	85/15
9	FePAM@T	1	2	100	100	100
10		2	2	100	100	100/0
11		3	2	37.4	28.8	77/23
12		3	4	100	80	80/20
13		4	4	43.3	33.2	76.5/23.5
14	PAM@M	1	1	0	0	0
15[b]	FePAM@M	1	1	100	100	100

[a] General conditions: G (0.18 mL, 2.50 mmol), acetone (0.84 mL, 11.41 mmol) and catalysts (8 mg, 0.4 mol% Fe respect to G, ratio Fe : G 1 : 250). [b] G (0.47 mL, 6.52 mmol), acetone (2.36 mL, 32.34 mmol) and catalysts (21 mg, 0.4 mol% Fe respect to G, ratio Fe : G 1 : 250). S = Solketal.

Measurements

The solid-state ^{13}C-NMR spectra were recorded using a Bruker AV-400-WB at room temperature and 100.32 MHz using a 4 mm triple channel probe using ZrO rotors and a Kel-F plug.

Microanalyses were carried out using a LECO CHNS-932 elemental analyzer (C, H, N).

FTIR-ATR spectra were obtained in a Bruker Vertex 70v with a resolution of 2 cm^{-1} and in the spectral range of 600–4000 cm^{-1}.

The thermal stability was evaluated *via* thermogravimetric analysis (TGA) using a TQ-500 from TA instruments. The thermograms were recorded under an air atmosphere at the heating rate of 10 °C min^{-1} from 50 to 800 °C.

Nitrogen adsorption isotherms were obtained using a Micromeritics ASAP 2020 M surface and porosity analyzer at 77 K. The samples were degassed for 12 h at 120 °C before taking measurements. Specific surface areas were determined using a BET technique.

X-ray powder diffraction patterns were recorded on a Bruker D8 diffractometer fitted with a Sol-X energy-dispersive detector. The instrument was operated at 40 kV and 30 mA, utilizing CuKα radiation (λ = 1.5418 Å) with appropriate filtering. Data were collected over a 2θ range of 3° to 50°, using a step size of 0.1° and an acquisition time of 0.5 seconds per step.

Results and discussion

Synthesis and characterization of poly(azomethine)s

Mechanochemical synthesis is a good alternative to obtain polymers mainly because it avoids or reduces the use of solvents, it can be used with low solubility monomers and, above all, it significantly shortens reaction times. However, it has been scarcely used for the synthesis of PAMs. Surprisingly, only one work has been published on the mechanochemical synthesis of PAMs, most likely due to the insolubility of the polymer in common solvents which greatly limits its applications.[18] However, for the use of PAMs as heterogeneous catalyst supports, insolubility is desired, and is indeed an essential requirement.

The synthesis of the PAM in this study was initially carried out *via* mechanochemical polymerization between the monomers 4,4′-diaminotriphenylamine (TPA) and 2,6-pyridinedicarboxaldehyde (DAPy) (Fig. 1a). The reaction was accomplished in the presence of a drying agent such as anhydrous magnesium sulphate with only 1 h of mechanical stirring at 600 rpm. Then, a dark brown solid insoluble in common solvents was formed, which was the first evidence of polymer growth. This polymer was designated as **PAM@M**. For comparative purposes, the reference poly(azomethine), was synthesized *via* a typical high-temperature polycondensation reaction through solution polymerization (Fig. 1b) using the same monomers. This polymer was designated as **PAM@T**. Pictures of both solids obtained are shown in Fig. S2.

The ^{13}C-NMR solid state spectra of both polymers (Fig. 2) showed similarities; however, the spectrum of **PAM@T** was

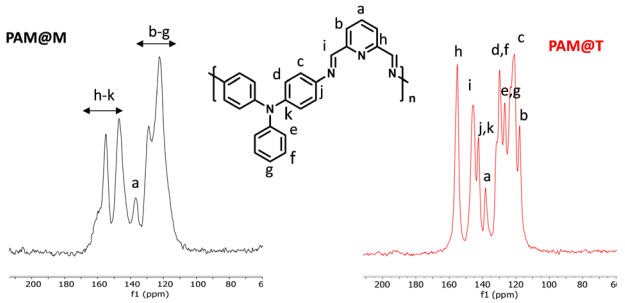

Fig. 2 ^{13}C-NMR solid state spectra of **PAM@M** and **PAM@T**.

notably more defined. The aromatic carbon atoms (a–g) showed signals between 110 and 140 ppm while carbons linked to nitrogen atoms exhibited chemical shifts at a lower field. Thus, the signal at 146 ppm is attributed to the imine carbon atoms (i) while the signals at 143 and 155 ppm are due to the aromatic carbon linked to nitrogen atoms, (j), (k) and (h) respectively.

To understand the differences in the spectral resolution between the two materials, the morphology of both polymers was studied *via* powder X-ray diffraction patterns (Fig. S3). The thermally synthesised **PAM@T** displays sharper Bragg reflections than mechanochemically synthesised **PAM@M**, indicating a higher degree of crystallinity. Consequently, a more ordered molecular structure contributes to the presence of more defined resonances in the solid-state ^{13}C NMR spectrum of **PAM@T**.[49,50]

Both polymers showed identical FT-IR absorption bands (Fig. 3a). The intense band at 1620 cm^{-1} was attributed to imine linkages. The absorption between 1578 and 1489 cm^{-1} was caused by the vibration of conjugated C=C bonds and the absorption attributed to C–N bonds occurred at 1411 cm^{-1}. Finally, a weak band at 1713 cm^{-1} was attributed to terminal aldehyde groups.[3]

Both PAMs showed a high thermal stability (Fig. 3b) with an initial decomposition temperature of 435 °C. Interestingly, the residual mass observed for **PAM@M** was higher than expected. This could be attributed to residual magnesium sulphate, tightly packed in the polymer matrix due to the mechanical action applied on the mixture, and which was not removed in the washing process. To verify this assumption, a TGA of pure $MgSO_4$ was performed under the same experimental conditions (Fig. S4). The analysis showed a high residual mass, consistent with the TGA profile observed for **PAM@M**. This supports the conclusion that the high residue in **PAM@M** is attributable to the presence of $MgSO_4$ in the final composite.

The percentages of C, H and N, obtained by elemental analysis (Table S1) were lower than expected due to the presence of the residual $MgSO_4$ trapped in this network. However, the elemental analysis values obtained for **PAM@T** were very similar to those calculated.

The monomers used to synthesize these polymeric supports, TPA and DAPy (Fig. 1), exhibit a *meta* disposition between their functional groups. This arrangement could give rise to a contoured structure with inherent porosity, a characteristic previously observed in other PAMs synthesized from monomers with similar functional group configurations.[3,21] Thus, we explored the porosity of both polymers using nitrogen adsorption/desorption isotherms at 77 K (Fig. S5). Neither polymer absorbs nitrogen at low pressures, indicating the absence of micropores in both structures. As pressure increases, both polymers absorb nitrogen, albeit in small amounts, resulting in very low specific surface areas of 18.3 and 24.9 m^2 g^{-1} respectively. **PAM@T** shows a very pronounced hysteresis, indicating that the nitrogen input and output are very different in this material, which can be attributed to the formation of very irregular pores with non-homogeneous size distribution. The **PAM@M** isotherm shows almost no hysteresis, indicating a more homogeneous distribution of pore size and shape. From these results it can be deduced that mechanochemical polymerization promotes the formation of pores that are more regular in shape and size.

Iron catalysts were prepared by heating a mixture of the corresponding PAM support with $FeCl_3$ in a polymer : metal salt molar ratio of 1 : 2 in methanol as the solvent. The metal content was determined after carrying out three thermogravimetric analyses (TGA) (Fig. 4a) under oxidizing atmosphere analysing the residue obtained (Fe_2O_3), that led to a medium iron contents of 5.46 ± 1.31 and 4.64 ± 0.25% respectively. These results together with the percentages of C, H and N obtained (Table S1) showed that one third of the repeating units of each catalysts anchor iron. The thermal stability was very similar in both cases, with a one-step decomposition pattern at similar initial degradation temperatures.

The FT-IR spectra of both complexes were also different (Fig. 4b). The **FePAM@M** spectrum shows a shift in the absorption of the imine bond from 1620 to 1601 cm^{-1} as a result of the

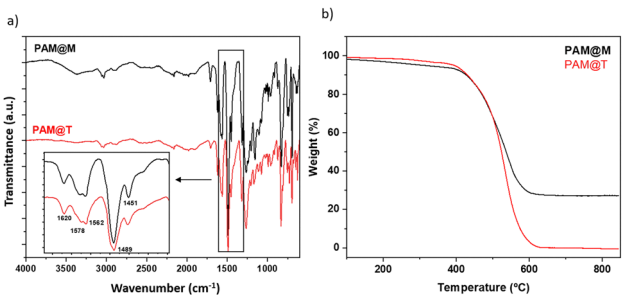

Fig. 3 (a) FT-IR spectra of **PAM@M** and **PAM@T**; (b) thermograms of **PAM@M** and **PAM@T**.

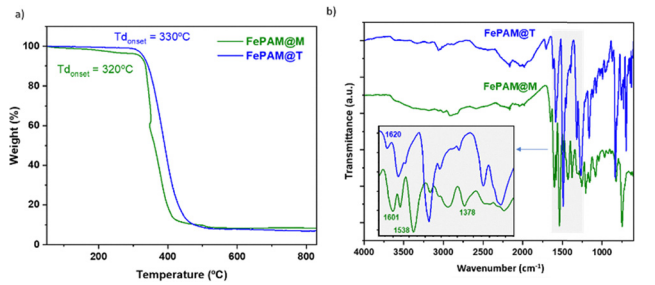

Fig. 4 (a) Thermograms and (b) FT-IR spectra of **FePAM@M** and **FePAM@T**.

coordination of iron cations to these bonds.[3] In addition, new absorptions appear in the spectrum of this complex at 1538 and 1378 cm^{-1} that were not present in the spectrum of the starting support (Fig. S6). However, the FT-IR spectrum of **FePAM@T** is very similar to that of the starting support (Fig. S7) which indicated that metal coordination in this case does not alter the vibrations of the bonds in this polymer. The different degrees of crystallinity in **PAM@M** and **PAM@T** may significantly influence the way the Fe-centre interacts with the polymer matrix at the molecular level. In the more amorphous **PAM@M**, less tightly packed chains and higher conformationally freedom, facilitate the Fe-coordination and thereby altering the corresponding IR bands, leading to observable shifts or intensity changes in IR bands. Conversely, in the more crystalline material **PAM@T**, the tighter packing and reduced segmental mobility can restrict the accessibility to surface positions of Fe ions where their dipole interaction is weak and the IR spectrum appears largely unchanged. This observation could suggest that the spectral response is governed by the local coordination environment.[51,52]

Glycerol valorisation

The acetylation of glycerol can produce two compounds, the five-membered ketal, solketal (S), and the six-membered ketal 2,2-dimethyl-1,3-dioxan-5-ol (DMDO) (Fig. 5). However, in most cases DMDO evolves to solketal which is thermodynamically more favourable.[53]

The reaction was optimized using **FePAM@M** as the catalyst. Thus, after several experiments, using an acetone/glycerol molar ratio of 7, and 0.4 mol% of iron respect to glycerol at room temperature, a complete conversion of glycerol into solketal, as the unique compound (100% yield and 100% selectivity) was achieved in only 1 hour of reaction (Table 1, entry 1). However, the use of **FePAM@T** under the same conditions did not yield complete glycerol conversion. It was necessary to increase the reaction time to 2 h to achieve complete conversion of glycerol and a quantitative yield in solketal (entry 9). The recycling of **FePAM@M** afforded the same results after two more consecutive reactions (entries 2 and 3, Fig. 6a). In the fourth cycle (entry 4), after 1 h of reaction, glycerol conversion was completed but a mixture of both acetals was detected. By increasing the reaction time to 2.5 h, DMDO was converted to solketal, which was the only product detected (entry 5). In the fifth cycle, the catalyst activity was lost since in one hour of reaction only 43% of the glycerol was reacted, forming a mixture of the two acetals (entry 6). Increasing the reaction time to 2.5 h, a mixture of 85% solketal and 15% DMDO was detected (entry 7). DMDO did not convert to solketal, as the same solketal/DMDO ratio was observed after 3.5 h of reaction (entry 8). In the case of FePAM@T (Fig. 6b), in the second cycle, glycerol conversion and solketal selectivity were 100% (entry 10) after 2 h of reaction. Then, in the third cycle, the glycerol conversion was 37.4% and a mixture of solketal and DMDO (77/23) (entry 11) was observed, which evolved towards 100% of glycerol conversion upon increasing the reaction time up to 4 h. In addition, the solketal yield increased to 80% (entry 12). The catalyst was deactivated in the fourth cycle since after four hours of reaction low glycerol conversion and loss of selectivity towards the solketal were observed (entry 13).

To confirm the role of iron, a control experiment was performed using **PAM@M** as the catalyst (entry 14). After 1 h of stirring at room temperature no reaction was observed, confirming the need for iron to promote this reaction. Finally, the reaction was up-scaled using **FePAM@M** as the catalyst (entry 15) to isolate solketal and calculate the *E*-factor (see the last paragraph of this section). As an example, Fig. S8 shows exemplary chromatograms of entries 1, 4 and 11 respectively.

The ^{1}H-NMR spectrum of solketal obtained without further purification (Fig. 7) shows expected signals: two singlets around 1.3 ppm attributed to the protons of methyl groups, a singlet at 2.7 assigned to the proton of the –OH moiety and a group of signals between 3.5 and 4.2 ppm attributed to the protons b–d.

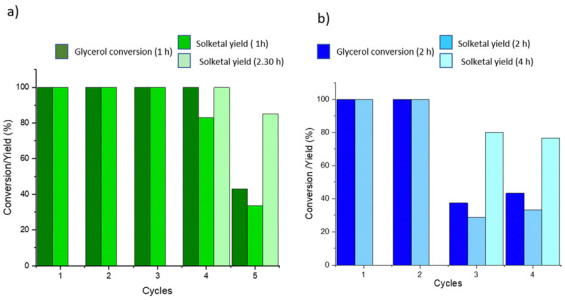

Fig. 6 Recycling experiments using (a) **FePAM@M** or (b) **FePAM@T** as catalysts.

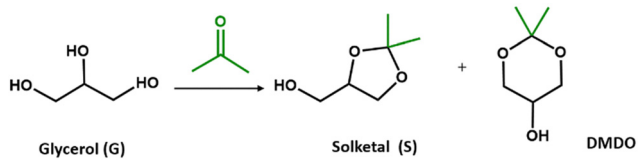

Fig. 5 Acetylation of glycerol.

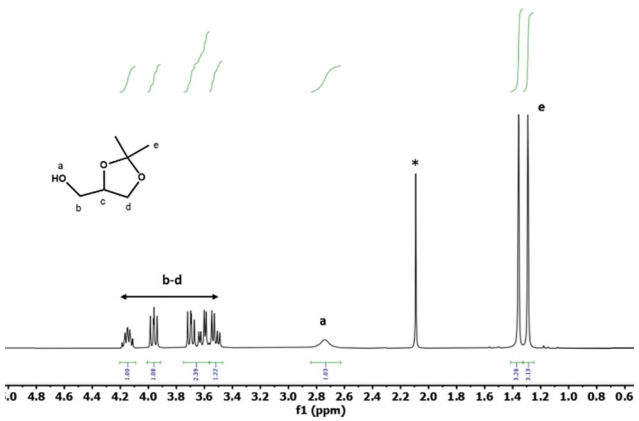

Fig. 7 ^{1}H-NMR spectrum of solketal prepared by acetylation of glycerol in 1 h at r.t. using **FePAM@M** as the catalyst (* acetone).

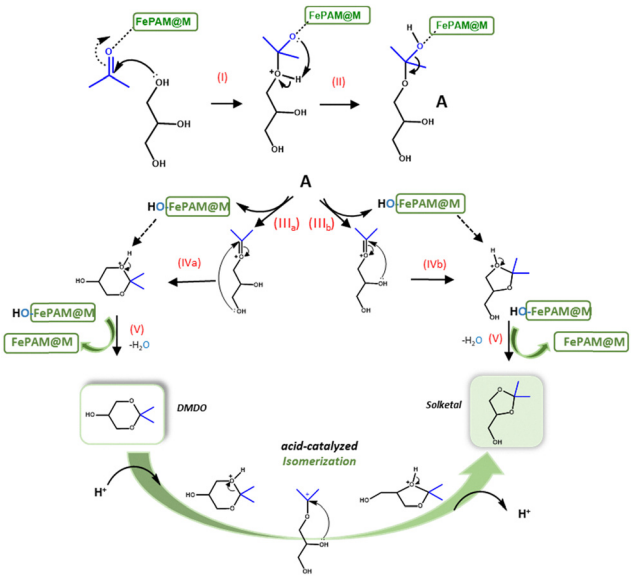

Fig. 8 Proposed mechanism for **FePAM@M**-catalyzed acetylation of glycerol to solketal.

The spectrum is consistent with that of commercial solketal and with that obtained by photocatalysis.[38]

The thermal stability of recycled-**FePAM@M** was compared with the catalyst before use (Fig. S9). The recycled catalyst shows a decrease in thermal stability (around 20 degrees) and a higher residue which confirms the lack of activity after the fourth cycle. The reduced thermal stability could be related to several factors such as a partial degradation of the polymeric structure during recycling processes, trace contamination by reaction by-products, or changes in the microstructure. These factors could affect the coordination of the iron complex, disrupt the polymer matrix, and consequently compromise thermal stability.

The glycerol acetylation mechanism to obtain solketal catalysed by **FePAM@M** is proposed in Fig. 8, based on other previously reported mechanisms using iron-loaded catalysts. The condensation reaction between alcohols and ketones begins with the activation of the carbonyl group through coordination with **FePAM@M**.[45,54] This activation facilitates the nucleophilic attack of the hydroxyl group on the carbonyl carbon (step I), forming a protonated tetrahedral alkyloxonium-like intermediate. Subsequently, this intermediate releases H^+ ions, which migrate to the oxygen atom coordinated with the catalyst (step II) to afford the intermediate **A**. The catalyst is then released (step III), generating a new oxyanion intermediate. This intermediate can undergo further transformation through a nucleophilic attack by a primary hydroxyl group (step IVa) or a secondary hydroxyl group (step IVb), leading to six- or five-membered ring intermediates, respectively. The formation of the five-membered ring is favoured due to the proximity between the secondary hydroxyl and carbonyl groups. Finally, a water molecule is eliminated, and the catalyst is regenerated (step V), yielding the two acetals, solketal and DMDO. However, DMDO is readily isomerized by an acid catalyst to solketal, the thermodynamically more stable product as has been previously reported.[55,56]

To provide an overview of the catalytic performance of **FePAM@M** in the valorisation of glycerol to solketal, it was compared with previously reported iron-loaded catalysts. Thus, Da Silva *et al.* achieved 96% solketal selectivity (98% glycerol conversion) in 1 h using 0.3 mol% of a recyclable homogeneous catalyst of iron(III) silicotungstate, which retained its activity over 5 cycles.[34] Ali *et al.* reported that using 5 wt% (with reference to the weight of glycerol) of a heteropoly ionic liquid-functionalized MOF-Fe, solketal is achieved with 100% selectivity with complete glycerol conversion in 1 h, retaining its activity over 7 cycles.[45] Thus, **FePAM@M** is very competitive to carry out this conversion, since very similar results are achieved even at room temperature in 1 h.

Finally, the process was evaluated in terms of chemical efficiency by calculating the *E*-factor (mass of waste/mass of product).[57] To determine this factor, the reaction was scaled up by increasing the amount of glycerol, acetone and **FePAM@M** as the catalyst (entry 15), which enabled the production of sufficient solketal for isolation and weighing (see the SI). The estimated value obtained was 3.49 which is even below that of the established waste segment in the chemical industry (5–50)[57] making this process highly sustainable and very attractive to apply on an industrial scale.

Conclusions

Mechanochemical polymerization was employed to synthesize a poly(azomethine)-type support (**PAM@M**) in only 1 h without the use of solvents, representing a significant advancement over traditional methods that typically require heating in solution for at least 24 h. The structure and chemical stability of **PAM@M** were comparable to those of the conventionally prepared counterpart (**PAM@T**). However, **PAM@M** demonstrated superior iron-anchoring capacity and enhanced catalytic activity in the acetylation of glycerol to produce solketal—a sustainable oxygenated fuel additive and eco-friendly alternative to petroleum-based additives. Notably, **FePAM@M** enabled full conversion of glycerol into solketal at room temperature in only 1 h, positioning it as a highly competitive catalyst on par with the best reported alternatives. Furthermore, the process is highly sustainable, with an *E*-factor of 3.49, making it particularly attractive for industrial-scale application. Thus, this research opens the way for exploring other metals supported on poly(azomethines) synthesized through mechanochemical polymerization, enabling the development of novel sustainable heterogeneous catalysts. Depending on the selected metal, these catalysts could be tailored for a wide range of chemical reactions, including those aimed at reusing waste, by-products or biomass conversions into optimized processes in the future.

Author contributions

J. A. Medina carried out the synthesis of PAM@M and iron-loaded catalysts, and began the studies of glycerol valorisation;

A. Matarín completed glycerol valorisation studies; P. A. Sobarzo carried out the synthesis of PAM@T, C. A. Terraza revised the manuscript and E. M. Maya was responsible for the work (conceptualization, funding acquisition, supervision and writing-original draft).

Conflicts of interest

There are no conflicts to declare.

Data availability

The data from this research will be available upon request.

The supplementary information file provides additional experimental details and characterization data supporting the findings reported in the main manuscript. It includes the synthetic procedure for 4,4′-diaminotriphenylamine (TPA), along with a calibration curve used for quantification (Fig. S1). Photographs of the PAM@M and PAM@T materials are shown in Fig. S2, while their structural properties are examined by X-ray powder diffraction (Fig. S3) and nitrogen adsorption–desorption isotherms (Fig. S5). Thermal stability is assessed *via* TGA of $MgSO_4$ (Fig. S4) and FePAM@M before and after recycling (Fig. S9). FT-IR spectra comparing FePAM@M and FePAM@T with their corresponding supports are provided in Fig. S6 and S7. Fig. S8 presents selected chromatograms related to the reaction products. Additionally, Table 1 contains elemental analysis data, and the E-factor calculation is included to evaluate the environmental impact of the process. See DOI: **https://doi.org/10.1039/d5ma00197h**

Acknowledgements

This research was funded by MICIU/AEI/10.13039/501100011033 FEDER, UE through the PID2023-146114NB-C22 project and FONDECYT grants 1230090 and 3220883. A. M. is grateful for the support received from the Interdisciplinary Platform for Sustainable Plastics towards a Circular Economy (SusPlast), CSIC.

Notes and references

1 A. Iwan, Z. Mazurak and D. Sek, *Polym. Eng. Sci.*, 2007, **47**, 1179–1186.
2 A. Iwan and D. Sek, *Prog. Polym. Sci.*, 2008, **33**, 289–345.
3 M. A. Brivary, M. Gómez, M. Iglesias and E. M. Maya, *J. Polym. Sci., Part A: Polym. Chem.*, 2018, **56**, 1946–1952.
4 E. M. Maya, M. González-Lucas and M. Iglesias, *ChemistrySelect*, 2017, **2**, 9516–9522.
5 J. L. Howard, Q. Cao and D. L. Browne, *Chem. Sci.*, 2018, **9**, 3080–3094.
6 T. Friščić, C. Mottillo and H. M. Titi, *Angew. Chem., Int. Ed.*, 2020, **59**, 1018–1029.
7 J.-L. Do and T. Friščić, *ACS Cent. Sci.*, 2017, **3**, 13–19.
8 S. L. James, C. J. Adams, C. Bolm, D. Braga, P. Collier, T. Friščić, F. Grepioni, K. D. M. Harris, G. Hyett, W. Jones, A. Krebs, J. Mack, L. Maini, A. G. Orpen, I. P. Parkin, W. C. Shearouse, J. W. Steed and D. C. Waddell, *Chem. Soc. Rev.*, 2012, **41**, 413–447.
9 L. Takacs, *Chem. Soc. Rev.*, 2013, **42**, 7649.
10 J. Haneef and S. Ali, *Sustainable Chem. Pharm.*, 2025, **45**, 102044.
11 F. Effaty, X. Ottenwaelder and T. Friščić, *Curr. Opin. Green Sustainable Chem.*, 2021, **32**, 100524.
12 D. V. Aleksanyan and V. A. Kozlov, *Mendeleev Commun.*, 2023, **33**, 287–301.
13 K. Kondo, K. Kubota and H. Ito, *Nat. Synth*, 2025, **4**, 744–753.
14 J. L. Howard, W. Nicholson, Y. Sagatov and D. L. Browne, *Beilstein J. Org. Chem.*, 2017, **13**, 1950–1956.
15 Y. Sim, Y. X. Shi, R. Ganguly, Y. Li and F. García, *Chem. – Eur. J.*, 2017, **23**, 11279–11285.
16 E. Boldyreva, *Chem. Soc. Rev.*, 2013, **42**, 7719.
17 Y. Nailwal, Q. Zhang, N. Brown, Z. Alsudairy, C. Harrod, M. H. Uddin, F. Akram, J. Li, Y. Liu and X. Li, *Chem. – Eur. J.*, 2025, **31**, e202500339.
18 S. Grätz and L. Borchardt, *RSC Adv.*, 2016, **6**, 64799–64802.
19 S. J. Pradeeba and K. Sampath, *Global NEST J.*, 2022, **24**, 407–413.
20 N. Yılmaz Baran, *J. Organomet. Chem.*, 2019, **899**, 120886.
21 P. A. Sobarzo, C. A. Terraza and E. M. Maya, *Eur. Polym. J.*, 2020, **126**, 109567.
22 E. M. Maya, E. Verde-Sesto, J. G. de la Campa and M. Iglesias, *ChemistrySelect*, 2016, **1**, 396–402.
23 J. Gaidukevič, J. Razumienė, I. Šakinytė, S. L. H. Rebelo and J. Barkauskas, *Carbon*, 2017, **118**, 156–167.
24 R. M. Kulkarni, P. J. Britto, A. Narula, S. Saqline, D. Anand, C. Bhagyalakshmi and R. N. Herle, *Biofuel Res. J.*, 2020, **7**, 1100–1108.
25 E.-E. Oprescu, E. Stepan, R. E. Dragomir, A. Radu and P. Rosca, *Fuel Process. Technol.*, 2013, **110**, 214–217.
26 H. Wang, H. Li, C. K. Lee, N. S. Mat Nanyan and G. S. Tay, *Int. J. Biol. Macromol.*, 2024, **261**, 129536.
27 N. Yadav, G. Yadav and M. Ahmaruzzaman, *Ind. Crops Prod.*, 2024, **210**, 117999.
28 M. J. Da Silva, A. A. Rodrigues and P. F. Pinheiro, *Fuel*, 2020, **276**, 118164.
29 L. Wang, X. Du, D. Zhang, T. Hu, D. Ren and Z. Huo, *ChemistrySelect*, 2024, **9**, e202400111.
30 P. Anastas and N. Eghbali, *Chem. Soc. Rev.*, 2010, **39**, 301–312.
31 F. G. Calvo-Flores, M. J. Monteagudo-Arrebola, J. A. Dobado and J. Isac-García, *Top. Curr. Chem.*, 2018, **376**, 18.
32 I. B. Laskar, K. Rajkumari, R. Gupta and S. L. Rokhum, *Energy Fuels*, 2018, **32**, 12567–12576.
33 F. Mirante, P. Leo, C. N. Dias, L. Cunha-Silva and S. S. Balula, *Materials*, 2023, **16**, 7023.
34 S. Maurya and Y. C. Sharma, *Fuel*, 2024, **355**, 129352.
35 B. Dashtipour, S. Dehghanpour and M. Sharbatdaran, *Polyhedron*, 2024, **247**, 116733.
36 G. H. M. Gomes, J. B. Gabriel, C. G. O. Bruziquesi, H. V. Victoria, K. Krambrock, L. C. A. Oliveira and N. D. S. Mohallem, *Ceram. Int.*, 2023, **49**, 14719–14732.
37 J. Martín-Gómez, M. Pérez-Losada, F. J. López-Tenllado, J. Hidalgo-Carrillo, M. C. Herrera-Beurnio, R. Estévez,

A. Marinas and F. J. Urbano, *Catal. Today*, 2024, **429**, 114506.
38 A. Matarín, L. González-Aguilera, M. L. Ferrer, M. Iglesias and E. M. Maya, *Solar RRL*, 2024, **8**, 2400304.
39 I. C. M. S. Santos-Vieira, R. F. Mendes, F. A. Almeida Paz, J. Rocha and M. M. Q. Simões, *Catal. Today*, 2023, **424**, 114296.
40 F. Drault, Y. Snoussi, J. Thuriot-Roukos, I. Itabaiana, S. Paul and R. Wojcieszak, *Catalysts*, 2021, **11**, 326.
41 H. Tokuyama, H. Suzuki, A. Terada and H. Ohashi, *React. Funct. Polym.*, 2023, **191**, 105697.
42 H. Tokuyama, H. Ohno and T. Fujita, *React. Funct. Polym.*, 2021, **165**, 104943.
43 S. K. Kundu, R. Singuru, T. Hayashi, Y. Hijikata, S. Irle and J. Mondal, *ChemistrySelect*, 2017, **2**, 4705–4716.
44 A. Talebian-Kiakalaieh, N. A. S. Amin, N. Najaafi and S. Tarighi, *Front. Chem.*, 2018, **6**, 573.
45 M. J. Da Silva, A. A. Rodrigues and M. G. Teixeira, *Energy Fuels*, 2020, **34**, 9664–9673.
46 A. L. G. Pinheiro, J. V. C. Do Carmo, D. C. Carvalho, A. C. Oliveira, E. Rodríguez-Castellón, S. Tehuacanero-Cuapa, L. Otubo and R. Lang, *Fuel Process. Technol.*, 2019, **184**, 45–56.
47 F. Mirante, P. Leo, C. N. Dias, L. Cunha-Silva and S. S. Balula, *Materials*, 2023, **16**, 7023.
48 C. O. Sánchez, J. C. Bèrnede, L. Cattin, M. Makha and N. Gatica, *Thin Solid Films*, 2014, **562**, 495–500.
49 K. Kato, T. Hiroi, S. Okada, S. Ohtani and T. Ogoshi, *Beilstein J. Org. Chem.*, 2025, **21**, 1183–1191.
50 A. M. Rose, A. R. McLauchlin, G. Wilson, T. O. McDonald and F. Blanc, *Polym. Chem.*, 2024, **15**, 1511–1521.
51 C. Castro, J. Ramos, A. Millán, J. González-Calbet and F. Palacio, *Chem. Mater.*, 2000, **12**, 3681–3688.
52 E. Meaurio, N. López-Rodríguez and J. R. Sarasua, *Macromolecules*, 2006, **39**, 9291–9301.
53 M. S. Vichare, M. Chakraborty and A. K. Jana, *Biomass Convers. Biorefin.*, 2024, **14**, 25637–25650.
54 A. A. Q. Ali and Z. N. Siddiqui, *Precision Chem.*, 2023, **1**, 485–496.
55 S. Ao and S. L. Rokhum, *J. Chem.*, 2022, **2022**, 1–18.
56 I. Zahid, M. Ayoub, M. H. Nazir, F. Sher, R. Shamsuddin, B. B. Abdullah and M. Ameen, *Biomass Bioenergy*, 2024, **181**, 107029.
57 R. A. Sheldon, *Green Chem.*, 2023, **25**, 1704–1728.